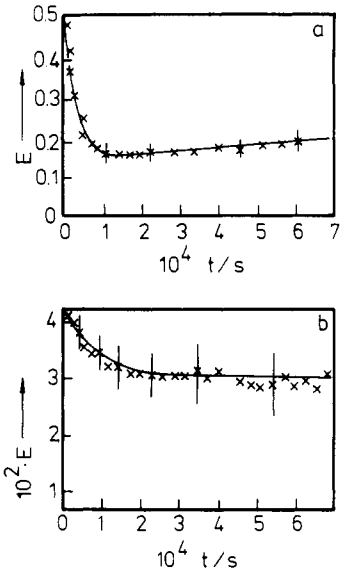

Figure 14. Simulation of absorption–time profiles for the experiment from Figure 2a (a) and Figure 2d (b).

Modelling of Observed Absorption–Time Profiles

Finally, the agreement between all measured absorption–time profiles and the modelled results on the basis of the shown rate and absorption coefficients will be demonstrated. Apart from the described absorption coefficients for benzyl iodide, benzyl radicals, dibenzyl, and benzyl fragments, and from the rate coefficients of eq 12–18, the modelling used literature values of $k_3 = 10^{11.75}$ exp(−14.6 kJ mol^{-1}/RT) and $k_4 = 10^{7.5}$ cm^3 mol^{-1} s^{-1} from ref 12 and 13, and of $k_5 = [\mathrm{Ar}]10^{13.99}$ exp(−127.2 kJ mol^{-1}/RT) cm^3 mol^{-1} s^{-1} and $k_5/k_6 = 10^{5.52}$ exp(−154 kJ mol^{-1}/RT) atm from ref 14 and 15. With these input data, for example, the absorption signals behind the incident and reflected wave in Figure 1f are reproduced as demonstrated in Figure 12. Figure 13 also shows the calculated concentration profiles of benzyl radical, molecular iodine, dibenzyl, and benzyl fragments behind the reflected shock wave for this experiment. The concentration dependence of the signals in Figure 2 is reproduced equally well as demonstrated with the simulated signals of Figure 14 for the experiments of Figure 2a,d. All other recorded profiles could be simulated in the same manner. Our simulations have always been accompanied by detailed sensitivity tests which are not reproduced here (for details, see ref 21). We, therefore, are confident that our analysis of the present experiments is complete and has led to a reliable characterization of the kinetic and spectroscopic properties of benzyl radicals under high-temperature conditions.

Acknowledgment. Financial support of this work by Deutsche Forschungsgemeinschaft is gratefully acknowledged.

Registry No. Benzyl iodide, 620-05-3; benzyl radical, 2154-56-5; benzyl chloride, 100-44-7; methyl benzyl ketone, 103-79-7.

(21) Müller-Markgraf, W. Ph.D. Dissertation, Göttingen, 1987.

Thermal Decomposition of Toluene: A Comparison of Thermal and Laser-Photochemical Activation Experiments

L. D. Brouwer, W. Müller-Markgraf, and J. Troe*

Institut für Physikalische Chemie der Universität Göttingen, Tammannstrasse 6, D-3400 Göttingen, West Germany *(Received: September 9, 1987; In Final Form: February 17, 1988)*

The thermal decomposition of toluene has been reinvestigated in shock waves detecting toluene, benzyl radicals, and benzyl fragment concentrations by UV absorption spectroscopy in the range 190–320 nm. The experiments are interpreted in terms of a dominant toluene dissociation into benzyl radicals + H fragments with a rate constant $k_1 = 10^{15.45\pm0.2}$ exp(−(371.9 ± 10) kJ mol^{-1}/RT) s^{-1} (at [Ar] = (2.6 ± 0.4) × 10^{-4} mol cm^{-3}) and in terms of a faster benzyl fragmentation which is in agreement with experiments on other benzyl sources. The derived thermally averaged rate constants of toluene dissociation k_1 are consistent with specific rate constants $k(E,J)$ from laser excitation experiments. Similarly, the nature of the dominant product channel is consistently identified in thermal and photochemical experiments, ruling out a recently discussed dominance of fragmentation into the phenyl + methyl channel.

Introduction

In spite of intense research over the past 10 years, the thermal decomposition of toluene under high-temperature combustion conditions still presents a series of puzzling uncertainties. Neither the rate of the primary fragmentation and the branching ratio into the two dissociation channels

$$C_7H_8\ (+M) \rightarrow C_7H_7 + H\ (+M) \qquad (1)$$

$$C_7H_8\ (+M) \rightarrow C_6H_5 + CH_3\ (+M) \qquad (2)$$

nor the mechanism of the subsequent reactions is well established. From a practical point of view, this situation is rather unfortunate since simple aromatic hydrocarbons constitute an increasing fraction of unleaded fuel for internal combustion engines. From a more fundamental point of view, laser-photochemical studies of vibrationally highly excited aromatic molecules present attractive opportunities for investigating model unimolecular bond fission processes.

Toluene dissociation has been studied over the temperature range 1500–2200 K in shock waves by a variety of detection techniques. UV absorption of the decomposing parent molecule and the forming benzyl radicals,[1-4] atomic resonance absorption of H atoms[5-7,10] (or D atoms in the case of deuterated toluene[5,6]), laser schlieren densitometry,[8] time-of-flight mass spectrometry,[8] and the single-pulse[9] technique have all been employed, leading

(1) Astholz, D. C.; Durant, J.; Troe, J. *Symp. (Int.) Combust., (Proc.), 18th* **1981**, 885.
(2) Astholz, D. C.; Troe, J. *J. Chem. Soc., Faraday Trans. 2* **1982**, *78*, 1413.
(3) Brouwer, L.; Müller-Markgraf, W.; Troe, J. *Symp. (Int.) Combust., (Proc.), 20th* **1984**, 799.
(4) Müller-Markgraf, W.; Troe, J. *Symp. (Int.) Combust., (Proc.), 21st* **1986**, 875.
(5) Rao, V. S.; Skinner, G. B. *J. Phys. Chem.* **1984**, *88*, 4362.
(6) Rao, V. S.; Skinner, G. B., submitted for publication in *J. Phys. Chem.*
(7) Frank, P.; Just, T. Poster presented at 21st Symposium (International) on Combustion, Munich, 1986.
(8) Pamidimukkala, K. M.; Kern, R. D.; Patel, M. R.; Wei, H. C.; Kiefer, J. H. *J. Phys. Chem.* **1987**, *91*, 2148.

0022-3654/88/2092-4905$01.50/0

to controversial interpretations even in the most recent work. This fact obviously is due to the complications from fast secondary reactions. In most studies, the dilution of the reactant was not high enough to avoid interference of the primary reaction with subsequent bimolecular reactions. With the most sensitive technique applied, i.e., atomic resonance absorption spectroscopy (ARAS), H atom production can originate not only from the primary dissociation but also from secondary fragments.[10-12] This complication is particularly serious in view of the recently established[4] unexpected short life of benzyl radicals C_7H_7 from eq 1. Since benzyl fragmentation is not understood in detail either, the interpretation of measurements employing relatively high toluene concentrations, such as laser schlieren experiments, remains preliminary and inconclusive due to mechanistic complications. VLPP[13] and Knudsen[14,15] mass spectrometric studies in part have reached up to the high temperatures considered and have led to useful complementary information but not resolved the basic difficulties.

In view of the limitations of thermal decomposition experiments, it appears useful to look for additional information about the primary fragmentation in photoexcitation experiments. Highly vibrationally excited electronic ground-state molecules of toluene have been prepared by $S_1 \rightarrow S_0^*$ internal conversion of electronically excited toluene after light absorption[16,17] or alternatively by unimolecular isomerization of cycloheptatriene after the analogous $S_0 + h\nu \rightarrow S_1 \rightarrow S_0^*$ preparation of the excited isomer.[18] UV absorption detection of the forming excited benzyl radicals[16-18] and hydrogen atoms[19,20] and mass-spectrometric detection of the branching into H atoms and CH_3 radicals in molecular beam experiments[21] were applied in laser flash excitation experiments. These "direct" studies of the fragmentation of toluene were not contaminated by secondary processes.

Considering the difficulties of the pyrolysis experiments, a combination of the nonthermal with thermal dissociation appears most helpful. It is the aim of the present article to present this analysis in the framework of unimolecular rate theory for simple bond fission processes. Before doing this, we describe a reinvestigation of toluene pyrolysis in shock waves using toluene and benzyl radical UV absorption measurements. On the basis of new information on benzyl radical absorption and fragmentation, we have undertaken a detailed modelling of the reaction mechanism with its possible complications. We then investigated to what extent the derived thermal dissociation rates are consistent with photoexcitation experiments. A discussion of the corresponding information on the branching ratio follows. Our study documents again the usefulness of a combination of thermal and nonthermal activation techniques.

Experimental Technique

Our experimental technique has been described in detail earlier.[1-4] Only a short summary will, therefore, be given here. Kinetic and spectroscopic studies were performed in incident and reflected shock waves using mixtures of toluene in Ar (dilution $[C_7H_8]/[Ar]$ = 15–1000 ppm), Ar total concentrations in the range 1×10^{-5} to 3×10^{-4} mol cm^{-3}, and temperatures of 1450–1900 K. Absorption profiles in the wavelength range 190–310 nm were recorded by using a pulsed Xe high-pressure arc lamp as the light source.

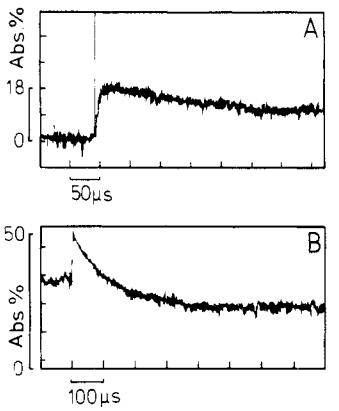

Figure 1. Thermal decomposition of toluene: (A) Time profile of the absorption of benzyl and benzyl fragments at λ = 257 nm (T = 1709 K, $[\text{toluene}]_{t=0} = 4.4 \times 10^{-9}$ mol cm^{-3}, $[Ar] = 3.1 \times 10^{-5}$ mol cm^{-3}; schlieren peak at the arrival of the reflected shock, absorption base line at 0). (B) Time profile of the absorption of toluene and benzyl fragments at λ = 190 nm (T = 1705 K, $[\text{toluene}]_{t=0} = 1.35 \times 10^{-9}$ mol cm^{-3}, $[Ar] = 3.0 \times 10^{-5}$ mol cm^{-3}; absorption behind the incident wave by toluene at T = 912 K, absorption base line at 0).

The observed absorption profiles stem from several species with broad overlapping absorption spectra. The parent molecule toluene at 1600 K has a broad absorption continuum which, at $\lambda \geq 190$ nm, decays monotonically with increasing wavelength.[22] Our recent study[4] of the high-temperature absorption spectrum of benzyl radicals shows much more structure with maxima of the spectrum of $\lambda \leq 190$ nm and at $\lambda \approx 230$, 260, and 310 nm. This spectrum extends toward longer wavelengths than that of toluene. Finally, the pyrolysis of benzyl radicals results in a broad "fragment spectrum" which again covers the whole range of wavelengths investigated, with an essentially monotonically decaying absorption coefficients at $\lambda > 190$ nm.[4] The overlap of these three spectra requires careful studies at various wavelengths and reaction conditions. Fortunately, at long wavelengths the signals are dominated by benzyl and "benzyl fragment" absorptions, whereas at short wavelengths mostly toluene and benzyl fragments contribute. Therefore, a separation of the different components of the absorption profiles becomes possible. This separation is greatly assisted by our separate studies of benzyl radicals from different precursor molecules.[4,23]

Experimental Results

Figure 1 compares typical absorption–time profiles at shorter and at longer wavelengths for a temperature near 1700 K. Both traces show a residual absorption signal due to benzyl fragments. On the other hand, the short-time signals at 190 nm indicate clearly the toluene decay, whereas at 257 nm (and likewise at 305 nm) the short-time profiles are dominated by benzyl appearance and disappearance. The early maximum of the 257-nm trace, compared to the decay of the 190-nm signal, suggests a rapid consumption of benzyl after its initial formation. This observation is in agreement with the determination of benzyl radical absolute concentrations which is possible now with the known benzyl radical absorption coefficient.[4,23] The quantitative evaluation of the initial rates of toluene dissociation and benzyl radical formation shows that they correspond to each other. However, since benzyl concentrations reach their maximum after about only 10% consumption of toluene, the initial rates cannot be analyzed very accurately. The rapid consumption of benzyl radicals and the low values of the absorption signals at 257 nm were not realized in ref 1–3 and are responsible for the incorrect interpretation of

(9) Colket, M. B.; Seery, D. J. Poster presented at 20th Symposium (International) on Combustion, Ann Arbor, MI, 1984.
(10) Braun-Unkhoff, M.; Frank, P.; Just, T. CEC Combustion Workshop, Abingdon, UK, Jan. 1987.
(11) Braun-Unkhoff, M.; Frank, P.; Just, T., private communication, 1987.
(12) Rao, V. S.; Skinner, G. B. *Symp. (Int.) Combust., (Proc.), 21st* **1986**, 809.
(13) Robaugh, D. A.; Stein, S. E. *Int. J. Chem. Kinet.* **1981**, *13*, 445.
(14) Smith, R. D. *J. Phys. Chem.* **1979**, *83*, 1553.
(15) Smith, R. D. *Combust. Flame* **1979**, *35*, 179.
(16) Brouwer, L.; Hippler, H.; Lindemann, L.; Troe, J., to be published.
(17) Ikeda, N.; Nakashima, N.; Yoshihara, K. *J. Chem. Phys.* **1985**, *82*, 5283.
(18) Hippler, H.; Schubert, V.; Troe, J.; Wendelken, H. J. *Chem. Phys. Lett.* **1981**, *84*, 253.
(19) Tsukiyama, K.; Bersohn, R. *J. Chem. Phys.* **1987**, *86*, 745.
(20) Ackermann, L. Ph.D. Thesis, Göttingen, 1982.
(21) Lee, Y. T., and co-workers, unpublished results cited in: Troe, J. In *Intramolecular Dynamics*; Jortner, J.; Pullmann, B., Eds.; Reidel: Dordrecht, 1982; p 311.
(22) Astholz, D. C.; Brouwer, L.; Troe, J. *Ber. Bunsenges. Phys. Chem.* **1981**, *85*, 559.
(23) Müller-Markgraf, W.; Troe, J. *J. Phys. Chem.*, preceding article in this issue.

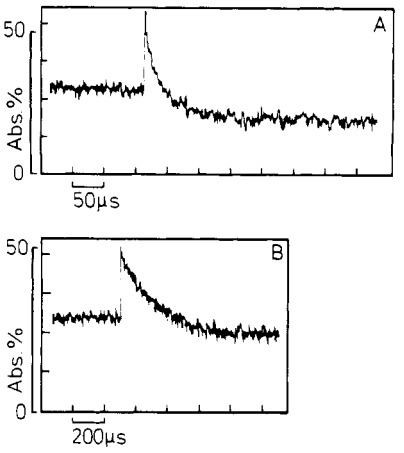

Figure 2. As in Figure 1, λ = 190 nm. (A) T = 1782 K, $[\text{toluene}]_{t=0}$ = 1.4 × 10^{-9} mol cm^{-3}, [Ar] = 2.7 × 10^{-5} mol cm^3. (B) T = 1626 K, $[\text{toluene}]_{t=0}$ = 1.4 × 10^{-9} mol cm^{-3}, [Ar] = 1.4 × 10^{-5} mol cm^{-3}.

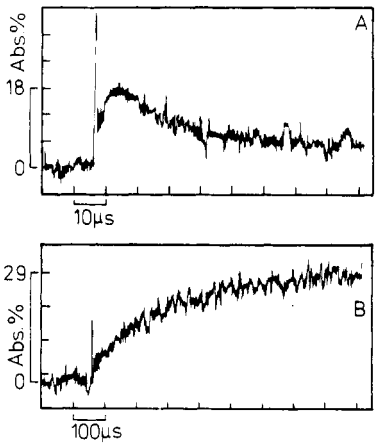

Figure 3. As in Figure 1, λ = 257 nm. (A) T = 1850 K, $[\text{toluene}]_{t=0}$ = 3.9 × 10^{-9} mol cm^{-3}, [Ar] = 2.7 × 10^{-5} mol cm^{-3}. (B) T = 1490 K, $[\text{toluene}]_{t=0}$ = 6.6 × 10^{-9} mol cm^{-3}, [Ar] = 3.1 × 10^{-5} mol cm^{-3}.

our earlier experiments. The two apparent rate constants of this earlier interpretation (the smaller for benzyl and the larger for toluene dissociation) now have to be inverted in order to account for the rapid approach of a benzyl maximum (see below).

The absorption profiles at 190 nm do not change their general appearance when the temperatures are changed, except for a marked temperature dependence of the decay time scale. Figure 2 demonstrates this behavior. It also shows the only slight changes of the residual absorption levels relative to the initial absorptions at this wavelength. The absorption profiles at 257 and 305 nm show a strong dependence of the benzyl rise time on temperature (see Figure 3). The time dependence does not correspond to an exponential rise profile. Furthermore, at temperatures high enough for the establishment of the final absorption level, a much stronger dependence of the residual absorption level on the temperature is observed than at 190 nm. It should also be mentioned that there is only a weak dependence of the observations on the initial concentration of toluene.

The evaluation of the observed absorption profiles relied on the three absorption coefficients (toluene, benzyl, and benzyl fragments) determined in separate experiments with undissociated toluene and different benzyl precursors. On the other hand, these absorption coefficients could also be treated as adjustable parameters and fitted to the present observations and the mechanism involved, (see below). Figure 4 and 5 show the resulting benzyl radical and benzyl fragment absorption coefficients which are fully consistent with our separate work on benzyl radicals (for the toluene spectrum at high temperatures, see ref 22 and 24; an

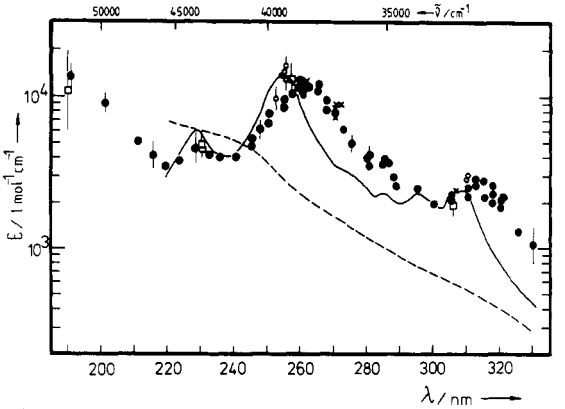

Figure 4. Absorption spectrum of benzyl radicals from the thermal decompositions of benzyl iodide[4,23] ((●) T = 1600 (±20) K, (○) 1160 (±30) K); toluene (this work, (□) 1600 K); and ethylbenzene[23] (×) 1600 K); (—) benzyl from laser flash photolysis of benzyl chloride,[43] $T \approx$ 1300 K; (---) phenyl from laser flash photolysis of chlorobenzene,[25] $T \approx$ 1400 K.

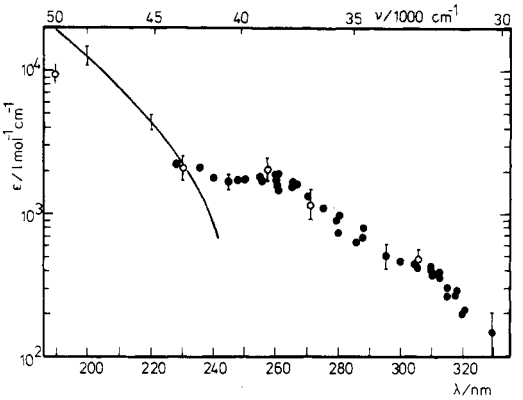

Figure 5. Absorption spectrum of benzyl fragments (see text) at T = 1600 K; precursors (●) benzyl iodide[4,23] and (○) toluene (this work). (—) Toluene absorption at T = 1600 K.

example is included in Figure 5). In the evaluation of the benzyl fragment absorption coefficient we assumed that benzyl decays into one absorbing, more stable, product. In reality, this evaluation can hide a variety of product species.

The evaluation of the concentration–time profiles was performed in several steps. At first, a simplified mechanism

$$C_7H_8 \rightarrow C_7H_7 + H \quad (1)$$

$$C_7H_7 \rightarrow \text{fragments} \quad (3)$$

of the A → B → C type was assumed which roughly represented our observations. Then the rate coefficients k_1 and k_3 and the absorption coefficients of the three species observed were fitted. Surprisingly, all observations (varying wavelengths, temperatures, and initial concentrations) could be reproduced fairly well by this simple mechanism. Nevertheless, there are clearly other reactions which can interfere with the simple mechanism. The influence of such reactions was investigated in large modelling and sensitivity tests as shown below. However, the final results hardly differed from the simple initial evaluation. In other works, our measurements apparently are sensitive to reactions 1 and 3, but not too much to other reactions. Since the primary formation of phenyl and methyl radicals via reaction 2 is also under discussion, phenyl and methyl spectra should be compared with the toluene, benzyl, and benzyl fragment spectra. Figure 4 includes the spectrum of hot phenyl radicals from chlorobenzene laser photolysis.[25] This spectrum is much weaker than that of benzyl. Even if the relatively low absorption signals at 257 and 305 nm (after

(24) Hippler, H.; Troe, J.; Wendelken, H. J. *J. Chem. Phys.* **1983**, *78*, 5351.

(25) Ikeda, N.; Nakashima, N.; Yoshihara, K. *J. Am. Chem. Soc.* **1985**, *107*, 3381.

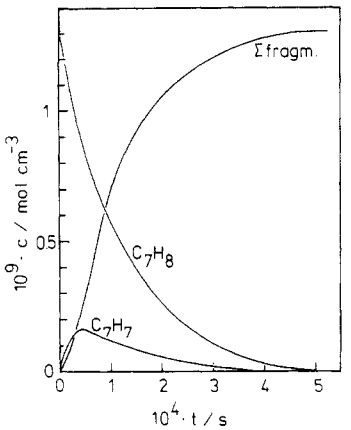

Figure 6. Calculated concentration–time profiles for the conditions of Figure 1 (from model B, see text; ∑fragm.: benzyl fragments).

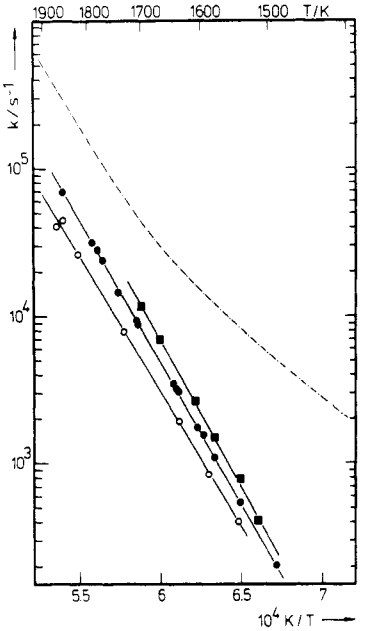

Figure 7. First-order rate coefficients for toluene decomposition (reaction 1) at (○) [Ar] = 1.05×10^{-5} mol cm^{-3}; (●) [Ar] = 3×10^{-5} mol cm^{-3}; (■) [Ar] = 2.6×10^{-4} mol cm^{-3}; (–·–·) rate coefficients for benzyl fragmentation (see Figure 8).

the maximum has been attained) were attributed to the weaker absorption by phenyl radicals, the strong initial rise of absorption in comparison to the toluene decay clearly would be in conflict with this hypothesis. There is the initial formation of a species which, at $260 \lesssim \lambda \lesssim 320$ nm, absorbs roughly 5 times stronger than phenyl radicals which we attribute to benzyl. Any absorption of phenyl, as well as of methyl radicals,[26] would be too weak to be detected in the presence of the stronger absorptions described before. The contributions of the three spectral components to the absorption–time profiles of Figures 1–3 can be constructed from the absorption coefficients of Figures 4 and 5 and the modelled concentration–time profiles such as shown in Figure 6 for the conditions of Figure 1.

As shown below, the present observables even when a large mechanism of secondary reactions is included can be interpreted well in terms of reactions 1 and 3 only. The results of this analysis of the absorption–time profiles are the absorption coefficients included in Figures 4 and 5 and the rate coefficients k_1 and k_3 shown in Figure 7 and 8. There appears to be a minor pressure dependence of k_1 in Figure 7. However, the scatter of the data is too large to be sure of this effect. Therefore, a construction of the falloff curve, such as given below, is required. The benzyl

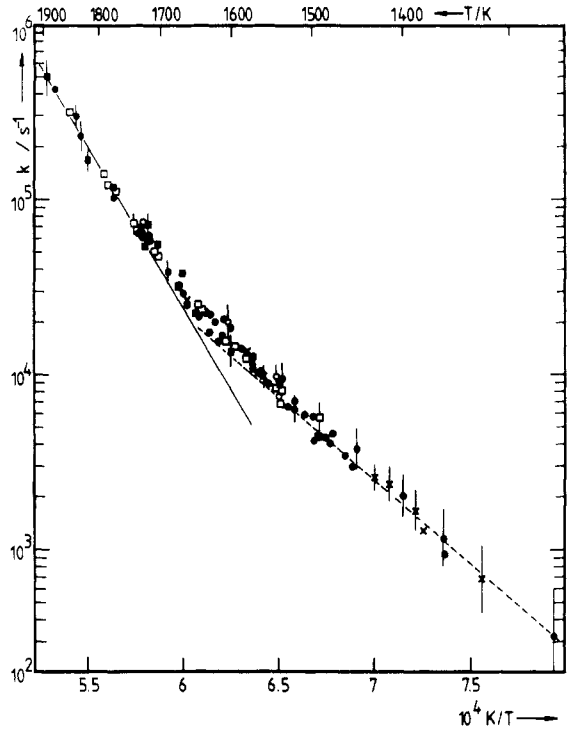

Figure 8. First-order rate coefficients for benzyl fragmentation (precursors (□) toluene from this work, (×) ethylbenzene, (●) benzyl iodide, (■) benzyl chloride, and (○) benzyl methyl ketone; see text).

radical fragmentation results in Figure 8 agree perfectly with observations from several other benzyl sources. Although the "unusual" temperature dependence of k_3 is not understood as yet,[4,12,14,15] the agreement of the various systems clearly confirms that genuine benzyl radicals were observed. The absorption signals definitely cannot be attributed to dominant phenyl radical formation.

Modelling of the Reaction Mechanism

In the following, the influence of a large variety of secondary reactions on the observed profiles of toluene, benzyl, and benzyl fragments is investigated. The mechanism was modelled and numerically solved by using a stiff-stable integrator routine of a modified Gear type.[27] Table I summarizes the reaction steps considered and the set of rate constants used. Sensitivity tests of the rate constants were also made with respect to the observed concentration profiles.

The following mechanistic models were treated in particular: We first undertook a modelling of the full mechanism of 38 reactions such as indicated in Table I (model A); we then compared the computed concentrations of model A with a calculation including only reactions 1, 3, 4, 5, and 6 (model B); i.e., a simplified model without fragmentation of benzyl fragments was considered. An even simpler model (model C) with only reactions 1, 3, and 4 served as the starting point of the experimental analysis (see above); a model with increased H production from benzyl fragments but no recombination was also considered, i.e., model A with $k_{22} = k_{23} = 0$ and $k_{21} = k_{24} = 10k_1$ (model D). Finally, the assumption of no production or consumption of H atoms from benzyl fragments was tested, i.e., model A with $k_{21} = k_{22} = k_{23} = k_{24} = 0$ (model E). A series of aspects of this modelling deserve particular emphasis. Our observations of absorption signals at 190 or 257 (and 310) nm, which are governed by toluene and benzyl fragment or benzyl radical and benzyl fragment contributions, are remarkably insensitive to the indicated model changes. Figure 9 shows examples of the simulated absorption–time profiles at 190 and 257 nm. There is hardly any difference between the models A, B, and D; model E (257 nm) shows some change, but only in the later stages of reaction. A crucial property of the

(26) Glänzer, K.; Quack, M.; Troe, J. *Symp. (Int.) Combust., (Proc.), 16th* **1977**, 949.

(27) Gear, C. W. *Comm. ACM* **1971**, *14* (3), 176, 185.

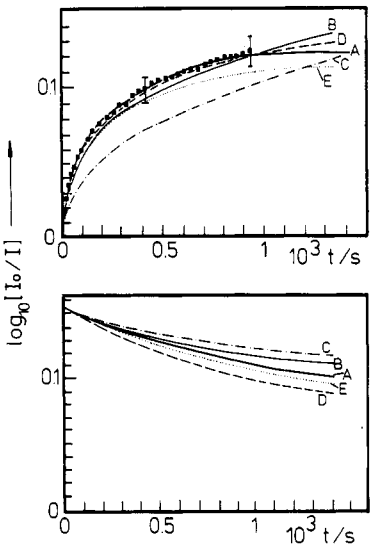

Figure 9. Calculated absorption–time profiles, see text. Upper diagram: λ = 257 nm, T = 1541 K, $[\text{toluene}]_{t=0} = 6.85 \times 10^{-9}$ mol cm^{-3}, [Ar] = 3×10^{-5} mol cm^{-3}, (■,▼) observed absorption–time profile; for models A–D, see text; calculations with ϵ(benzyl) = 1×10^4 L mol^{-1} cm^{-1}, ϵ(benzyl fragments) = 1.8×10^3 L mol^{-1} cm^{-1}. Lower diagram: λ = 190 nm, T = 1541 K, $[\text{toluene}]_{t=0} = 6.85 \times 10^{-10}$ mol cm^{-3}, [Ar] = 3×10^{-5} mol cm^{-3}, observed absorption–time profile coinciding with model A; calculations with ϵ(toluene) = 2.25×10^4 L mol^{-1} cm^{-1}, ϵ(benzyl) = 1.1×10^4 L mol^{-1} cm^{-1}, ϵ(benzyl fragments) = 9.8×10^3 L mol^{-1} cm^{-1}.

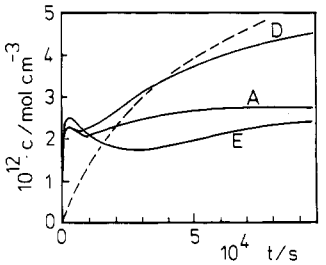

Figure 10. Calculated H atom profiles $c(t)$ using models A, D, E for T = 1540 K, $[\text{toluene}]_{t=0} = 6.85 \times 10^{-9}$ mol cm^{-3}, [Ar] = 3×10^{-5} mol cm^{-3}. (---) Measured H atom profile[5] at T = 1478 K, $[\text{toluene}]_{t=0}$ = 1.39×10^{-10} mol cm^{-3}, [Ar] = 2.8×10^{-5} mol cm^{-3}.

present mechanism is the higher rate of disappearance of benzyl radicals as compared to toluene. This key phenomenon has been verified independently with all different benzyl precursor molecules and thus appears unambiguous. It is this property which was unexpected in the incorrect interpretation of our earlier experiments.[1-3] The neglect of the H + benzyl recombination (5) was suggested in ref 8 to be responsible for the misinterpretation. However, this suggestion is not valid since the toluene ⇌ benzyl + H equilibrium is depleted by rapid benzyl removal. Surprisingly, the ultrasimplified model C omitting the H + benzyl (5) and H + toluene (6) reactions gives practically the same results as the simple models B (at least at shorter wavelengths and/or lower initial concentrations) including these steps, and the complete model A. The reason is found in a compensating effect: varying k_5 and k_6 for constant ratio k_5/k_6 has only little influence; however, independent variations of k_5 and k_6 show somewhat larger effects. Since the ratio k_5/k_6 is fairly well established, the present use of model B instead of model A in the data analysis is justified.

The observed toluene, benzyl, and benzyl fragment profiles are fairly insensitive to the large number of known or unknown reactions following benzyl or phenyl fragmentation. This is not the case for profiles of H atoms and later products such as C_2H_2 and CH_4. Figure 10 demonstrates calculated H atom profiles for models A, D, and E at the conditions of an experiment from ref 5; Figure 11 shows C_2H_2 and CH_4 profiles from model A for experiments from ref 8. These profiles are all much more sensitive to the rate parameters of secondary reactions which have only little influence on the observations of our present work. We are,

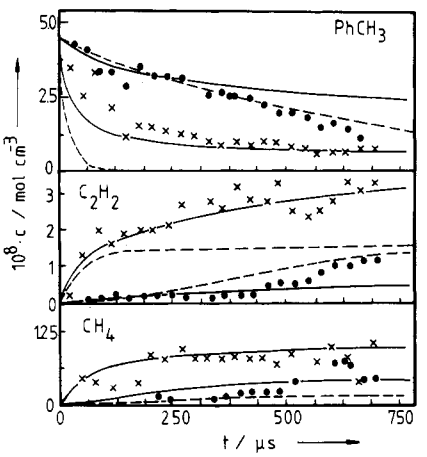

Figure 11. Time-of-flight mass-spectrometric measurements[8] of toluene ($PhCH_3$), C_2H_2, and CH_4 profiles at T = 1590 K (●) and 1832 K (×). (—) Model calculations from ref 8 ($[\text{toluene}]_{t=0} \approx 4.6 \times 10^{-8}$ mol cm^{-3}); (---) calculations for model A from this work ($[\text{toluene}]_{t=0} = 4.5 \times 10^{-8}$ mol cm^{-3}).

therefore, presently not concerned about the unsatisfactory results for CH_4 and H profiles. Some of the relevant secondary reactions were included in our modelling. There will be certainly more of such processes which are not yet understood.

Sensitivity tests with the rate parameters of Table I showed dominant sensitivity with respect to k_1 and $k_3 + k_4$, and a minor sensitivity to the ratio k_5/k_6. The perfect consistency between the behavior of benzyl radicals in the toluene system and in other clearly benzyl-forming systems like benzyl chloride and ethylbenzene, as well as the observations on the benzyl spectrum and other arguments (see below), rule out a major contribution from the high-energy fragmentation pathway toluene → phenyl + methyl (2). There would be no way to reproduce all of the present observations if a dominant dissociation via reaction channel (2) were assumed. From our sensitivity analysis we estimate the ratio k_2/k_1 to be smaller than 0.3. The final results of the present analysis, therefore, are rate coefficients k_1, k_3, and k_4 such as given in Figures 7 and 8 and Table II . Uncertainties due to experimental scatter and influences from mechanistic complications are estimated to be of the order ±20%. (It should be emphasized that we primarily derive $k_3 + k_4$. A separation is attempted only on the basis of the break in the temperature dependence; see Figure 8.)

Theoretical Analysis of Specific and Thermally Averaged Rate Constants for Toluene Dissociation

It was emphasized in the Introduction that thermal dissocation experiments for toluene have to be compared with energy-selective photoexcitation experiments. The observed rate coefficients of the two excitation modes have to be consistent with each other. A realistic theoretical interpretation allows one to construct falloff curves which are required for a meaningful evaluation of the thermal dissociation experiments. Furthermore, information on the branching into different primary product channels from photoexcitation experiments can be applied to the interpretation of the thermal dissociation experiments.

In recent years we have experimented with various versions of statistical unimolecular rate theory in order to find the most economical approach. Since simple bond fission processes are concerned, the problem of rotational effects in the specific rate constants $k(E,J)$ has to be treated with particular care. Room temperature photoexcitation experiments are characterized by different rotational distributions than high-temperature thermal dissociation experiments. There may also be rotational effects in the shape of the falloff curves. Conventional RRKM theory with oscillator-type activated complexes will not be adequate for this purpose. In principle, the RRKM code could be fitted to the experimental falloff curves and high-pressure rate constant k_∞; however, the reconstruction of the relevant specific rate constant $k(E,J)$ for photoexcitation, because of the rotational effects, will

TABLE I: Mechanism for Toluene Pyrolysis[a]

	log A	E_a/kJ mol^{-1}	reference
1. $PhCH_3 \rightarrow PhCH_2 + H$	15.3	369.1	present work [Ar] = 3 × 10^{-5} mol cm^{-3}
2. $PhCH_3 \rightarrow Ph + CH_3$	$k_2 \approx k_1/10$		21
3. $PhCH_2 \rightarrow C_5H_5 + C_2H_2$	10.22	187	23, present work [Ar] = 3 × 10^{-5} mol cm^{-3}
4. $PhCH_2 \rightarrow C_4H_4 + C_3H_3$	15.3	349.6	23, present work [Ar] = 3 × 10^{-5} mol cm^{-3}
5. $PhCH_2 + H \rightarrow PhCH_3$	13.9–14.9	0	20, 42, present work
6. $PhCH_3 + H \rightarrow PhCH_2 + H_2$	$A = 10^{-4.12}T^{5.5}$	1.422	5
7. $2PhCH_2 \rightarrow PhCH_2CH_2Ph$	12.7	1.93	23
8. $PhCH_2CH_2Ph \rightarrow 2PhCH_2$	14.9	250	23
9. $PhCH_2CH_2Ph + H \rightarrow PhCHCH_2Ph + H_2$	12–13	0	estimated
10. $PhCHCH_2Ph \rightarrow PhCHCHPh + H$	15.9	217	estimated, 46
11. $PhCH_3 + H \rightarrow Ph + CH_4$	$k_{11} \approx k_{16}/100$		14, 15
12. $PhCH_3 + CH_3 \rightarrow PhCH_2 + CH_4$	12.4–12.6	0	47
13. $Ph \rightarrow C_4H_3 + C_2H_2$	15.08	343	48
14. $C_6H_6 \rightarrow Ph + H$	15.7	227.2	49
	16.76	244.35	49, k_∞
15. $C_6H_6 \rightarrow C_4H_4 + C_2H_2$	14.11	368.2	48
16. $PhCH_3 + H \rightarrow C_6H_6 + CH_3$	13.08	21.43	50
17. $C_6H_6 + H \rightarrow Ph + H_2$	13.45	66.9	48
18. $2Ph \rightarrow PhPh$	12.3–12.7	0	estimated
	11.4		51
19. $PhPh \rightarrow 2Ph$	15.5	390	estimated
20. $C_5H_5 \rightarrow C_3H_3 + C_2H_2$	15.0	167.4	9, estimated in ref 52
21. $C_5H_5 \rightarrow C_5H_4 + H$	0–3.8 at 1541 K		see text, see also ref 12
22. $C_5H_5 + H \rightarrow C_5H_6$ } 23. $C_3H_3 + H \rightarrow C_3H_4$ }	0–13.0		depending on pressure and applied model, see text
24. $C_4H_4 \rightarrow C_4H_3 + H$	11.3	251	53, see text
25. $C_4H_4 \rightarrow 2C_2H_2$	13.0	334.7	48
26. $C_4H_4 \rightarrow C_4H_2 + H_2$	13.0	305.4	48
27. $C_4H_3 \rightarrow C_4H_2 + H$	11.3	213.4	48
28. $C_4H_3 + H \rightarrow C_4H_2 + H_2$	14.3	60.7	48
29. $C_4H_4 + H \rightarrow C_4H_3 + H_2$	14.48	60.7	
30. $2CH_3 \rightarrow C_2H_6$	13	0	26, [Ar] = 3 × 10^{-5} mol cm^{-3}
	13.21	0	54, 55, [Ar] = 3 × 10^{-5} mol cm^{-3}
31. $C_2H_6 \rightarrow 2CH_3$	15.85	356	56, p = 6.3 atm
	15.36	347.7	56, p = 1.7 atm
32. $C_2H_6 \rightarrow C_2H_5 + H$	15.5	340	estimated
33. $C_2H_6 + H \rightarrow C_2H_5 + H_2$	13.2	38.5	57
34. $CH_3 + H \rightarrow CH_4$	$A = 10^{26.90+\log[Ar]}/T^3$	0	58
35. $CH_4 + H \rightarrow CH_3 + H_2$	14.9	62.6	59
36. $CH_4 \rightarrow CH_3 + H$	17.67	390	59, k_∞
	12.67	389.2	59, p = 1.6 atm
37. $C_2H_6 + CH_3 \rightarrow C_2H_5 + CH_4$	13.3	44.4	estimated
38. $C_2H_5 \rightarrow C_2H_4 + H$	12.95	159	60, k_∞
	13.5	170.3	51

[a] Representation $k = A \exp(-E_a/RT)$; A in s^{-1} or cm^3 mol^{-1} s^{-1}; Ph = C_6H_5.

TABLE II: Measured Rate Coefficients of Reactions 1, 3, and 4 from This Work

$k_1 = 10^{14.6} \exp(-353.5 \text{ kJ mol}^{-1}/RT)$ s^{-1} at [Ar] = 1.05 (±0.1) × 10^{-5} mol cm^{-3}
$k_1 = 10^{15.3} \exp(-369.1 \text{ kJ mol}^{-1}/RT)$ s^{-1} at [Ar] = 3.0 (±0.3) × 10^{-5} mol cm^{-3}
$k_1 = 10^{15.45} \exp(-371.9 \text{ kJ mol}^{-1}/RT)$ s^{-1} at [Ar] = 2.6 (±0.4) × 10^{-4} mol cm^{-3}
k_3[a] $= 10^{10.22} \exp(-187.0 \text{ kJ mol}^{-1}/RT)$ s^{-1} and $k_4 = 10^{15.3} \exp(-349.6 \text{ kJ mol}^{-1}/RT)$ s^{-1} at [Ar] = 3.0 (±0.3) × 10^{-5} mol cm^{-3}

[a] Tentative separation of the benzyl fragmentation rates from Figure 8 into k_3 and k_4.

not necessarily be satisfactory. Our approach in terms of the statistical adiabatic channel model (SACM)[28] interpolates between "rigid" RRKM and "loose" phase space theory (PST). In this way rotational effects are automatically included. Various simplified versions[29-31] have been tested in applications to simple bond fissions of much smaller molecules.[29-32] It should be emphasized that these versions of the theory are still based on crude representations of the potential energy surface of the reaction. Future improvements of the theory are in the direction of implementing more realistic potentials, done either in the framework of variational transition-state theory[33,34] by using Montecarlo sampling of the phase space[33] or by explicit constructions of adiabatic channel eigenvalues for a given potential.[35] These approaches are not yet in a state where they could be applied economically to a problem of the present complexity. Therefore, in the following we construct specific rate constants $k(E,J)$, thermally averaged rate constants k_∞, and falloff curves employing simplified SACM in the versions of ref 29–31.

Our approach involves the choice of a parameter α/β, i.e., the ratio of a "looseness parameter" α and the Morse parameter β, fitted in such a way that $k(E,J)$ and k_∞ are represented in a

(28) Quack, M.; Troe, J. *Ber. Bunsenges. Phys. Chem.* **1974**, *78*, 240.
(29) Troe, J. *J. Chem. Phys.* **1981**, *75*, 226.
(30) Troe, J. *J. Chem. Phys.* **1983**, *79*, 617.
(31) Brouwer, L.; Cobos, C. J.; Troe, J.; Dübal, H. R.; Crim, F. F. *J. Chem. Phys.* **1987**, *86*, 6171.
(32) Cobos, C. J.; Hippler, H.; Troe, J. *J. Phys. Chem.* **1985**, *89*, 342, 1778. Cobos, C. J.; Hippler, H.; Luther, K.; Ravishankara, A. R.; Troe, J. *J. Phys. Chem.* **1985**, *89*, 4332.
(33) Wardlaw, D. M.; Marcus, R. A. *Chem. Phys. Lett.* **1984**, *110*, 230; *J. Chem. Phys.* **1985**, *83*, 3462; *J. Phys. Chem.* **1986**, *90*, 5383.
(34) Hase, W. L.; Mondro, S. L.; Duchovic, R. J.; Hirst, D. M.; *J. Am. Chem. Soc.* **1987**, *109*, 2916.
(35) Troe, J. *J. Phys. Chem.* **1986**, 90, 3485; *Chem. Phys. Lett.* **1985**, *122*, 425; *J. Chem. Phys.* **1987**, *87*, 2773.

TABLE III: Molecular Parameters for Modelling Toluene Bond Fission

toluene frequencies (in cm^{-1}): 3085, 3070, 3058, 2920, 1604, 1493, 1378, 1208, 1176, 1028, 1002, 784, 524, 973, 841, 406, 983, 893, 734, 690, 467, 217, 3037, 3028, 2950, 1548, 1455, 1455, 1331, 1313, 1153, 1080, 1040, 620, 347, one free internal rotor with effective rotational constant 5.37 cm^{-1}, from ref 61–63

benzyl frequencies (in cm^{-1}): 3060, 3060, 3050, 2860, 1600, 1480, 1330, 1270, 1160, 1010, 980, 810, 520, 950, 820, 360, 980, 890, 750, 640, 420, 170, 3030, 3040, 2930, 1550, 1440, 1440, 1350, 1300, 1160, 1070, 600, 610, 360, from ref 64–67

toluene rotational constants (in cm^{-1}): 0.189, 0.084, 0.0583
benzyl rotational constants (in cm^{-1}): 0.189, 0.0906, 0.0613 from ref 63, 68, 69

reaction coordinate (in cm^{-1}): 2979
disappearing oscillators (in cm^{-1}): 1455, 1040
correlations for transitional modes (in cm^{-1}): 1455 ↔ 0.189, 1040 ↔ 0.0906, 0.189 ↔ 0.0613; correlation for internal rotor, 5.37 ↔ 290 cm^{-1}

threshold energy ΔH_0° = 361 ± 6 kJ mol^{-1} ≅ 30180 cm^{-1} from ref 70, 71

effective symmetry numbers: toluene σ = 6, benzyl σ = 2

parameters for quasi-triatomic representation of centrifugal energy (eq 3.10 and 3.11 from ref 29): a_1 = 0.01794, a_2 = 0.00231

consistent manner. The limitation to a minimum number of fit parameters in the past always proved to be satisfactory. The universality and the existence of a semiquantitative relation between the potential surface and the ratio α/β allowed for predictions and interpretations of many reaction systems.[36] A choice of $\alpha/\beta \approx 0.5$ is a reasonable start for the modelling, before a fine tuning of this parameter is done by comparison with experiments.

Table III summarizes the sets of reactant (toluene) and product (benzyl) vibrational frequencies and rotational constants, the correlations of disappearing reactant oscillators with product rotors, and other calculational parameters. We use the simplified version of the SACM from ref 30 in order to calculate $k(E,J)$. The high-pressure rate constants k_∞ are then derived by thermal averaging of $k(E,J)$ over E and J, or by using the corresponding canonical version of the theory.[29] Because of the coupling of "transitional modes" (or "disappearing oscillators") with the use of slightly different coupling relations (expressed by effective Morse parameters $\beta_{eff}(E,J)$ and $\beta_{eff}(T)$), the two treatments are not completely consistent. However, in the present applications the two approaches gave results which, for the same α/β, agreed within 10–20%. We also applied the improved treatment of the coupling in terms of improved $\beta_{eff}(E,J)$ expressions of ref 31. However, in the present case no major effects were observed. The present treatment of the limiting phase space theory (and the resulting angular momentum correction factors $F_{AM\infty}(E,J)$ involved accurate counting of rovibrational numbers of open channels $W_1(E^*,J)$ by treating the dissociation fragments as a spherical top and an atom (eq C 20 and C 21 of ref 30). Since explicit analytical expressions are available here, the simplified interpolations between low-J and high-J expressions could be abandoned. The $W_1(E^*,J)$ for transitional modes were then convoluted with conserved oscillators using the Beyer-Swinehart counting algorithm.[37]

Because of the simplified character of the treatment, numerical artifacts have to be looked for. In our recent analysis of H_2O_2 fragmentation,[31] simplified and detailed SACM were compared. Although slightly different α/β ratios were fitted by the two approaches, the same $k_\infty \Leftrightarrow k(E,J)$ relationships were obtained. This is what is required for the present application. Actually, only the simplified SACM was elaborated. However, a comparison with the SACM-modified phase space theory proposed in ref 31 and 38 will also be given.

(36) Cobos, C. J.; Troe, J. *J. Chem. Phys.* **1985**, *83*, 1010.
(37) Astholz, D. C.; Troe, J.; Wieters, W. *J. Chem. Phys.* **1979**, *70*, 5107.

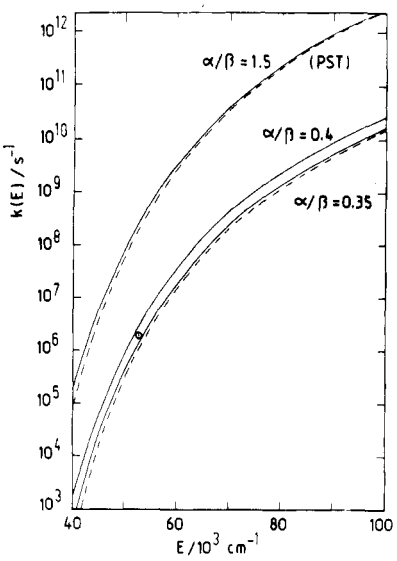

Figure 12. Specific rate constants $k(E,J)$ for toluene dissociation into benzyl + H (see Table IV; (—) J = 0, (– – –) J = 100, intermediate J values between the two curves; E indicates vibrational plus rotational energy; (⊙) laser experiment for $\langle J \rangle$ = 38 from ref 16 and 18).

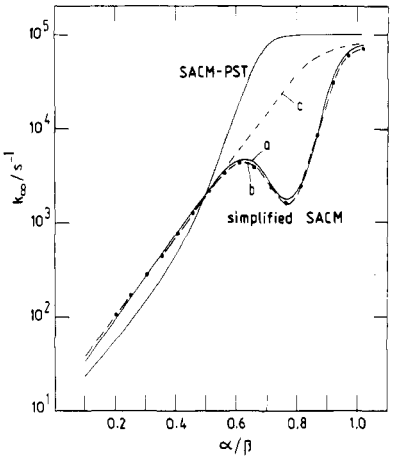

Figure 13. Thermally averaged high-pressure rate constants k_∞ for toluene dissociation at T = 1500 K. (Simplified SACM: (a) thermal averaging of microcanonical specific rate constants $k(E,J)$ from Table IV (ref 30); (b) canonical version of the model from ref 29; (c) empirical correction of curve a. SACM–PST: SACM-modified phase space calculations from ref. 31, 38).

Figure 12 and Table IV shows specific rate constants $k(E,J)$ for different values of the ratio α/β in comparison to the limit given by phase space theory (PST) which corresponds to $\alpha/\beta \gtrsim 1$. Ratios α/β smaller than unity introduce rigidity into the treatment such that the rate constants become considerably smaller than given by PST. Thermal averaging leads to the corresponding k_∞ such as documented in Figure 13. The simplified SACM expresses "quanta" ϵ and number of channel exponents x as a function of α/β in an empirically fitted way (see eq 3.18 and 3.22 from ref 29). For $\alpha/\beta > 0.5$, i.e., for results close to the PST limit $\alpha/\beta \gtrsim 1$, these equations (from ref 29) can produce x values below the PST-limiting value 0.5 for a certain range of α/β. This artifact is responsible for the observed inflection of the $k_\infty(\alpha/\beta)$ curve in Figure 13. The SACM-modified PST of ref 31 which fixes x to 0.5 avoids this artifact. Calculating effective rotational constants $B_{eff} = (\epsilon_1\epsilon_2)^{1/2}$ of the benzyl fragment such as given in Table V, this approach results in $k_\infty(\alpha/\beta)$ curves also shown in Figure 13. For $\alpha/\beta \leq 0.5$, the two approaches give similar results and should be free from this artifact. In reality, for $\alpha/\beta \approx 0.5$, we use the simplified SACM result (curve a in Figure 13) which is consistent with the $k(E,J)$ curves in Figure 12. The decrease of the

(38) Troe, J. *J. Chem. Phys.* **1986**, *85*, 1708.

TABLE IV: Specific Rate Constants $k(E,J)$ for Toluene Dissociation into Benzyl + H[a]

	$J = 0$			$J = 10$			$J = 40$			$J = 100$		
E	$\alpha/\beta = 0.35$ $E_0(J) =$ 30250	$\alpha/\beta = 0.4$ $E_0(J) =$ 30180	$\alpha/\beta = 1.5$ $E_0(J) =$ 30180	$\alpha/\beta = 0.35$ $E_0(J) =$ 30250	$\alpha/\beta = 0.4$ $E_0(J) =$ 30190	$\alpha/\beta = 1.5$ $E_0(J) =$ 30180	$\alpha/\beta = 0.35$ $E_0(J) =$ 30340	$\alpha/\beta = 0.4$	$\alpha/\beta = 1.5$ $E_0(J) =$ 30250	$\alpha/\beta = 0.35$ $E_0(J) =$ 30820	$\alpha/\beta = 0.4$	$\alpha/\beta = 1.5$ $E_0(J) =$ 30700
30 300	1.0×10^{-6}	4.5×10^{-6}	9.5×10^{-4}	7.2×10^{-7}	3.1×10^{-6}	9.3×10^{-4}		9.2×10^{-8}	5.5×10^{-5}			
30 400	3.6×10^{-6}	1.1×10^{-5}	1.9×10^{-3}	3.6×10^{-6}	1.0×10^{-5}	1.9×10^{-3}	4.0×10^{-7}	3.2×10^{-6}	7.7×10^{-4}			
30 500	7.5×10^{-6}	2.1×10^{-5}	3.4×10^{-3}	7.4×10^{-6}	2.0×10^{-5}	3.4×10^{-3}	2.6×10^{-6}	9.0×10^{-6}	1.7×10^{-3}			
30 700	2.5×10^{-5}	6.9×10^{-5}	1.0×10^{-2}	2.5×10^{-5}	6.5×10^{-5}	1.0×10^{-2}	1.2×10^{-5}	3.3×10^{-5}	5.8×10^{-3}			3.5×10^{-6}
31 000	1.1×10^{-4}	2.7×10^{-4}	3.8×10^{-2}	1.1×10^{-4}	2.6×10^{-4}	3.8×10^{-2}	5.9×10^{-5}	1.6×10^{-4}	2.4×10^{-2}	1.8×10^{-6}	6.3×10^{-5}	1.4×10^{-3}
32 000	3.2×10^{-3}	7.7×10^{-3}	9.8×10^{-1}	3.2×10^{-3}	7.4×10^{-3}	9.8×10^{-1}	2.2×10^{-3}	5.4×10^{-3}	7.3×10^{-1}	3.3×10^{-4}	8.5×10^{-4}	1.3×10^{-1}
33 000	3.9×10^{-2}	5.8×10^{-2}	1.1×10^{1}	3.9×10^{-2}	8.3×10^{-2}	1.1×10^{1}	2.9×10^{-2}	6.3×10^{-2}	8.6×10^{0}	7.0×10^{-3}	1.6×10^{-2}	2.4×10^{0}
35 000	1.6×10^{0}	3.3×10^{0}	3.9×10^{2}	1.6×10^{0}	3.3×10^{0}	3.9×10^{2}	1.3×10^{0}	2.7×10^{0}	3.4×10^{2}	4.7×10^{-1}	1.0×10^{0}	1.4×10^{2}
37 000	2.5×10^{1}	3.5×10^{1}	5.8×10^{3}	2.5×10^{1}	5.1×10^{1}	5.8×10^{3}	2.1×10^{1}	4.5×10^{1}	5.2×10^{3}	9.9×10^{0}	2.1×10^{1}	2.6×10^{3}
40 000	5.9×10^{2}	1.2×10^{3}	1.5×10^{5}	5.9×10^{2}	1.2×10^{3}	1.3×10^{5}	5.1×10^{2}	1.1×10^{3}	1.2×10^{5}	3.0×10^{2}	6.2×10^{2}	7.2×10^{4}
45 000	2.7×10^{4}	5.2×10^{4}	5.4×10^{6}	2.7×10^{4}	5.2×10^{4}	5.4×10^{6}	2.5×10^{4}	4.9×10^{4}	5.1×10^{6}	1.7×10^{4}	3.3×10^{4}	3.7×10^{6}
50 000	4.2×10^{5}	8.0×10^{5}	8.4×10^{7}	4.2×10^{5}	7.9×10^{5}	8.0×10^{7}	4.0×10^{5}	7.6×10^{5}	7.7×10^{7}	3.0×10^{5}	5.8×10^{5}	6.1×10^{7}
52 000	1.0×10^{6}	1.9×10^{6}	2.0×10^{8}	1.0×10^{6}	1.9×10^{6}	2.0×10^{8}	9.9×10^{5}	1.9×10^{6}	1.9×10^{8}	7.7×10^{5}	1.5×10^{6}	1.5×10^{8}
55 000	3.5×10^{6}	6.5×10^{6}	6.3×10^{8}	3.4×10^{6}	6.4×10^{6}	6.3×10^{8}	3.3×10^{6}	6.2×10^{6}	6.2×10^{8}	2.7×10^{6}	5.0×10^{6}	5.2×10^{8}
60 000	1.9×10^{7}	3.4×10^{7}	3.3×10^{9}	1.9×10^{7}	3.4×10^{7}	3.3×10^{9}	1.8×10^{7}	3.3×10^{7}	3.9×10^{9}	1.5×10^{7}	2.8×10^{7}	2.8×10^{9}
70 000	2.4×10^{8}	4.1×10^{8}	4.0×10^{10}	2.3×10^{8}	4.1×10^{8}	4.0×10^{10}	2.3×10^{8}	4.0×10^{8}	3.9×10^{10}	2.0×10^{8}	3.6×10^{8}	3.6×10^{10}
80 000	1.4×10^{9}	2.5×10^{9}	2.4×10^{11}	1.4×10^{9}	2.5×10^{9}	2.4×10^{11}	1.4×10^{9}	2.4×10^{9}	2.4×10^{11}	1.3×10^{9}	2.2×10^{9}	2.2×10^{11}
90 000	5.6×10^{9}	9.4×10^{9}	8.9×10^{11}	5.6×10^{9}	9.4×10^{9}	9.0×10^{11}	5.6×10^{9}	9.2×10^{9}	8.9×10^{11}	5.1×10^{9}	8.7×10^{9}	8.5×10^{11}
100 000	1.6×10^{10}	2.6×10^{10}	2.5×10^{12}	1.6×10^{10}	2.6×10^{10}	2.5×10^{12}	1.6×10^{10}	2.5×10^{10}	2.5×10^{12}	1.5×10^{10}	2.4×10^{10}	2.4×10^{12}

[a] All energies in units of cm^{-1}.

TABLE V: Effective Quanta ϵ and Exponents x for Transition Modes in Toluene Dissociation[a]

α/β	ϵ_1	x_1	ϵ_2	x_2	ϵ_3	x_3
0.1	655.8	(0.883)	449	(0.883)	0.12	(0.5)
0.2	287	(0.779)	187	(0.780)	0.09	(0.5)
0.3	114	(0.688)	70.6	(0.686)	0.07	(0.5)
0.35	67.7	(0.643)	40.5	(0.646)	0.07	(0.5)
0.4	37.3	(0.605)	21.4	(0.601)	0.06	(0.5)
0.5	8.50	(0.513)	4.38	(0.525)	0.06	(0.5)
0.6	1.26	(0.421)	0.56	(0.436)	0.06	(0.5)
0.7	0.25	(0.343)	0.11	(0.329)	0.06	(0.5)
0.8	0.19	(0.340)	0.09	(0.290)	0.06	(0.5)
0.9	0.19	(0.426)	0.09	(0.428)	0.06	(0.5)
1.0	0.19	(0.488)	0.09	(0.497)	0.06	(0.5)

[a] 1, transition mode 1455 → 0.189 cm^{-1}; 2, transition mode 1040 → 0.089 cm^{-1}; 3, transition mode 0.189 → 0.06 cm^{-1}, calculation following ref 29.

TABLE VI: Reduced Falloff Curve for Toluene Dissociation at T = 1700 K[a]

k_0/k_∞	F^{WC}	k/k_∞	k_0/k_∞	F^{WC}	k/k_∞
2×10^{-1}	0.65	0.0093	2×10^{4}	0.79	0.74
2×10^{0}	0.68	0.041	2×10^{5}	0.80	0.80
2×10^{1}	0.71	0.14	2×10^{6}	0.82	0.82
2×10^{2}	0.74	0.34	2×10^{7}	0.83	0.83
2×10^{3}	0.76	0.58			

[a] Weak collision broadening factors F^{WC} are included,[39] using $\beta_c \approx 0.04$, see text. The center of the falloff curve, i.e., $k_0/k_\infty = 1$, corresponds to $[Ar]_{cent} \approx 3 \times 10^{-9}$ mol cm^{-3}.

SACM–PST curve in Figure 13 below curve a) for $\alpha/\beta \approx 0.5$ is due to an increase of x to values above 0.5 (see Table V). Under these conditions, therefore, the SACM–PST model becomes inappropriate. The optimum correction of Figure 13 is obtained by an empirical bridging of the artificial inflection of the curves a and b, such as done in curve c of Figure 13.

Fixing an optimum value of the effective ratio α/β is performed in a sequence of operations. With a first choice of $\alpha/\beta \approx 0.5$, a falloff curve including rotational effects is constructed. This is then applied to the thermal dissociation result such that k_∞ is deduced. Figure 13 indicates the corresponding ratio α/β, and Figure 12 leads to $k(E,J)$. For the relevant energy and angular momentum distribution at room temperature an average $\langle k(E,J)\rangle_J$ is also estimated and compared with photoexcitation results. A fine tuning of the ratio α/β improves the fit to the two sets of experiments and controls the internal consistency.

The falloff curve of the thermal dissociation is calculated at first in the strong collision approximation. Falloff expressions for fixed J are derived and then averaged over the relevant rotational distributions. Additional weak collision broadening of the falloff curve is then applied as described in ref 39. Because of the markedly lower k_∞ obtained by the revised interpretation, falloff curves are now obtained which, for the experimental pressures, are closer to the high-pressure limit compared to our first construction of falloff curves in ref 1. Around [Ar] = 10^{-5}–10^{-4} mol cm^{-3}, the strong collision falloff curves show only a few percent falloff of k below k_∞. Table VI documents the corresponding calculations of reduced falloff curves. However, there is probably a pronounced weak collision broadening. At present not enough is known about the relevant energy-transfer properties at high temperatures (see the limited experimental studies in ref 40). Nevertheless, assuming a temperature-independent value of the collision efficiency $\beta_c \approx 0.04$ (because of large F_E values, see ref 39), one estimates the broadening effects included in Table VI. According to this construction, at the [Ar] concentrations employed and the corresponding great distance from the center of the falloff curves, weak collision broadening dom-

(39) Troe, J. *Ber. Bunsenges. Phys. Chem.* **1983**, *87*, 161. Gilbert, R. G.; Luther, K.; Troe, J. *Ber. Bunsenges. Phys. Chem.* **1983**, *87*, 169.

(40) Heymann, M.; Hippler, H.; Troe, J. *J. Chem. Phys.* **1984**, *80*, 1853. Heymann, M.; Hippler, H.; Plach, H. J.; Troe, J. *J. Chem. Phys.* **1987**, 87, 3867.

inates over strong collision broadening. Flat falloff curves result with $k/k_\infty \approx 0.8$ at $T \approx 1700$ K and [Ar] $\approx 10^{-4}$ mol cm^{-3}. With this still somewhat uncertain falloff construction, our final result for the high-pressure rate constant of toluene C–H bond fission becomes

$$k_\infty \approx 10^{15.2\pm0.3} \exp(-\Delta H_0^\circ / RT)\ \text{s}^{-1}$$

where $\Delta H_0^\circ = 361$ kJ mol^{-1}. According to Figure 13, the derived thermally averaged k_∞ value is fitted by an α/β ratio of about 0.35. From this, the corresponding specific rate constants $k(E,J)$ follow as given by Figure 12 and Table IV. In room temperature photoexcitation experiments, probably the initial energy and angular momentum distribution of the molecules during the light absorption is conserved. Identifying the measured dissociation rate constant[16-18] $k(E) \approx 1.9\ (\pm0.1) \times 10^6$ s^{-1} with the specific rate constant at average thermal energy (plus the photon energy) and average angular momentum (i.e., $\langle J \rangle \approx 38$ and $\langle E \rangle = \langle E_{\text{vib}} \rangle + \langle E_{\text{rot}} \rangle + h\nu \approx (680 + 310 + 51730)$ cm^{-1} = 52 720 cm^{-1} for irradation of toluene at $\lambda = 193.3\ (\pm0.7)$ nm), one may compare photoexcitation and thermal dissociation results. According to Figures 12 and 13, there is agreement within about 30% between the results. The general uncertainties of measurements, mechanistic interpretation, and theoretical modelling probably are of the order of a factor of 2. Within this uncertainty, thermal dissociation and energy-selective photolysis, therefore, are fully consistent with each other.

Discussion

In the following we summarize and discuss observations and arguments in favor and against the present interpretation of toluene fragmentation rates and products. These pieces of information stem from thermal and photochemical activation systems in combination with statistical unimolecular rate theory.

(i) The UV absorption measurements of toluene and benzyl radicals in the present work provide a direct access to toluene and benzyl fragmentation rates. Uncertainties in the large number of secondary reactions shown in Table I have only little influence on the derived rate constants. The benzyl fragmentation rates obtained agree with the corresponding rates in other benzyl reaction systems such as the pyrolysis of benzyl iodide, benzyl chloride, benzyl methyl ketone, and ethylbenzene. It appears highly improbable that these different systems do not lead to genuine benzyl properties.

(ii) The benzyl radical spectra, absolute absorption coefficients, and wavelength dependence, derived from toluene dissociation, agree with those derived from the other benzyl precursors mentioned in (i). Within the scatter of the data (±20%) they indicate a yield of at least 70% benzyl from toluene primary bond fission.

(iii) The thermal rate constant k_1 derived from toluene disappearance and benzyl radical appearance rates is fully consistent with the toluene fragmentation rate measured under collision-free conditions after laser excitation.[16-18] The detailed theoretical modelling of the specific and thermally averaged rate constants given above proves this consistency in a convincing way. This is independent of possible artifacts of unimolecular rate theory.[31]

(iv) The dissociation rate constant k_1 is also fully consistent with measurements of the reverse thermal recombination H + benzyl → toluene (5). Such measurements include pulse radiolysis[41] and laser flash photolysis[20,42] ($k_5 \approx 1.7 \times 10^{14}$ cm^3 mol^{-1} s^{-1} at 300 K from ref 41, 42, and 20). Although there are some uncertainties in the equilibrium constant $K = k_1/k_5$ due to incomplete knowledge of the benzyl internal rotation barrier, the agreement between K and k_1/k_5 within a factor of 2 appears certain.[8]

(v) The benzyl radical absorption spectrum from thermal dissociation experiments agrees fairly well (see Figure 4) with hot benzyl spectra from laser photolysis of benzyl chloride.[43] Some minor differences are due to the not so well-defined "temperature" of benzyl radicals in this photolysis system. Unfortunately, due to the overlap of hot toluene and benzyl spectra, a similar conclusion cannot be obtained from toluene laser photolysis. However, after collisional cooling, laser photolysis of toluene leads to genuine cool benzyl radicals with complete conversion (within ±10%) of toluene into benzyl.[16] The cool spectra of the products in benzyl chloride and toluene photolysis agree perfectly. It would be highly improbable that toluene dissociation rates after thermal and photochemical excitation are fully consistent and the dissociation products were not.

(vi) Molecular beam photofragment spectra of toluene after laser excitation have also confirmed dominant H atom over CH_3 production.[21] A branching ratio $k_2/k_1 \approx 0.1$ (upper limit 0.3) was derived.

(vii) H atom formation rates in the photoexcitation of cycloheptatriene with subsequent isomerization into hot toluene were found to be fully consistent with toluene dissociation rates.[19]

(viii) The phenyl + CH_3 channel of toluene dissociation is considerably more endothermic than the benzyl + H channel. The coupling of the two channels in the falloff range due to weak collision effects discriminates against the high-energy channel. Although this effect becomes smaller close to the high-pressure limit, it is present.[44]

The arguments (i)–(viii) appear to provide an overwhelming evidence in favor of the present results and interpretation. Recent arguments in favor of dominant toluene fragmentation into the phenyl channel (2) from laser schlieren experiments,[8] or at least of a 1:1 contribution of reactions 1 and 2 from atomic resonance absorption measurements,[6] have to be analyzed carefully. Some points to consider are raised in the following.

(ix) Recent measurements of H profiles in ref 7, 10, and 11 confirm very well the toluene dissociation rates from the present study. In the modelling, alternatively dominant reactions 1 or 2 were considered. The observed H-profiles clearly favored dominant benzyl formation. However, since the contribution of H atoms from genuine benzyl fragmentation is not well understood as yet, and H atoms are strongly influenced by several of the "later reactions" shown in Table I (see above), more studies with different benzyl sources are necessary before unique interpretations are possible.

(x) Laser schlieren studies favor reaction 2 over reaction 1 because of the fast fragmentation of phenyl radicals. The same effect on the density gradient can be produced by fast fragmentation of benzyl radicals such as shown in our work. The laser schlieren technique cannot distinguish between these two alternatives. Reference 8 argues against the possibility of a fast benzyl decay referring to our old benzyl decomposition rates which, as shown now, have to be exchanged with the toluene decomposition rates. Whereas this argument clearly does not apply any longer, inconsistencies with benzyl formation in laser schlieren experiments of ethyl benzene decompostion[45] are also mentioned. However,

(41) Pagsberg, P.; Sillesen, O.; Troe, J., to be published.
(42) Löhmannsröben, H. G. Diploma Thesis, Göttingen, 1981. Luu, S. H.; Glänzer, K.; Troe, J. *Ber. Bunsenges. Phys. Chem.* **1975**, *79*, 855.
(43) Ikeda, N.; Nakashima, N.; Yoshihara, K. *J. Phys. Chem.* **1984**, *88*, 5803.
(44) Just, T.; Troe, J. *J. Phys. Chem.* **1980**, *84*, 3068.
(45) Mizerka, L. J.; Kiefer, J. H. *Int. J. Chem. Kinet.* **1986**, *18*, 363.
(46) Brooks, C. T.; Peakock, S. J.; Reuben, B. R. *J. Chem. Soc., Faraday Trans. 1* **1982**, *78*, 3187.
(47) Litzinger, T. A.; Brezinsky, K.; Glassman, I. *Combust. Flame* **1986**, *63*, 251.
(48) Kern, R. D.; Wu, C. H.; Skinner, G. B.; Rao, V. S.; Kiefer, J. H.; Towers, J. A.; Mizerka, L. J. *Symp. (Int.) Combust., (Proc.), 20th* **1984**, 789.
(49) Hsu, D. S. Y.; Lin, C. Y.; Lin, M. C. *Symp. (Int.) Combust., (Proc.), 20th* **1984**, 626.
(50) Robaugh, D.; Tsang, W. *J. Phys. Chem.* **1986**, *90*, 4159.
(51) Benson, S. W.; O'Neil, H. E. "Kinetic Data on Gas Phase Unimolecular Reactions"; *Natl. Stand. Ref. Data Ser. (U.S., Natl. Bur. Stand.)* **1970**, No. 21.
(52) Pamidimukkala, K. M.; Kern, R. D. *Int. J. Chem. Kinet.* **1986**, *18*, 1341.
(53) Kiefer, J. H.; Shah, J. N., private communication, 1986.
(54) Arthur, N. L. *J. Chem. Soc., Faraday Trans. 2* **1986**, *82*, 331.
(55) McPherson, T.; Pilling, M. J.; Smith, M. J. C. *Chem. Phys. Lett.* **1983**, *4*, (94), 430.
(56) Burcat, A.; Skinner, G. B.; Crossley, R. W.; Scheller, R. *Int. J. Chem. Kinet.* **1975**, *5*, 343.
(57) Herron, J. T. *Int. J. Chem. Kinet.* **1969**, *1*, 527.

again mechanistic complications in the ethyl benzene mechanism can easily be made responsible for the laser schlieren observations. Fast benzyl fragmentation with H formation and a competition with benzyl + H → toluene combination, as well as other reactions, complicate the situation. Since benzyl fragmentation is not understood in detail (and we are far from this at present), the laser schlieren experiments do not appear direct enough to allow for a unique analysis of the complicated mechanism.

(xi) The present work does not give much insight into the later reactions governing final product formation such as provided to a greater extent by mass spectrometry[14,15] and single-pulse shock experiments.[8] There are only two points to be raised here. The mechanism of ref 8 involves formation of benzyl and methylphenyl isomers. The latter are assumed to be much less stable than benzyl radicals. The estimated decomposition rates of methylphenyl are close to the present benzyl decomposition rates. This may suggest that there is essentially only one C_7H_7 species involved. One may also argue that the experiments are completely insensitive to reaction 1, because of the fast recombination H + benzyl, such that reaction 2 dominates the overall reaction. However, in the presence of a fast benzyl consumption by other processes this argument can be ruled out on the basis of the present mechanistic modelling. Clearly, the fragmentation of benzyl provides the key for a further understanding of the system.

In summary one may state that the comparison of thermal and photochemical dissociation rates of toluene now presents a clear picture of the primary bond fission process. There appears to be clear indication of dominant C–H bond fission with well-established specific and thermally averaged rate constants. More work needs to be done in order to understand details of the fragmentation of benzyl radicals.

Acknowledgment. Financial support of this work by the Deutsche Forschungsgemeinschaft as well as calculational help by P. Borrell and collaboration with L. Lindemann on laser experiments are gratefully acknowledged.

Registry No. C_7H_8, 108-88-3; C_7H_7, 2154-56-5; $PhCH_2CH_2Ph$, 103-29-7; H, 12385-13-6; $PhCHCH_2Ph$, 36877-87-9; Ph, 2396-01-2; PhPh, 92-52-4; C_2H_6, 74-84-0; CH_3, 2229-07-4.

(58) Warnatz, J. In *Chemistry of Combustion Reactions*, Gardiner Jr., W. C., Ed.; Springer: New York, 1984.
(59) Roth, P.; Just, T. *Ber. Bunsenges. Phys. Chem.* **1975**, *79*, 682.
(60) Trenwith, A. B. *J. Chem. Soc., Faraday Trans. 2* **1986**, *82*, 457.
(61) Dempster, A. B.; Powell, D. B., Sheppard, N. *Spectrochim. Acta* **1975**, *31A*, 245.
(62) Hitchcock, A. P.; Laposa, J. D. *J. Mol. Spectrosc.* **1975**, *54*, 223.
(63) Rudolph, H. D.; Dreizler, H.; Jäschke, A.; Wending, P. *Z. Naturforsch* **1967**, 22a, 940.
(64) Lutoshkin, V. J.; Kotorlenko, L. A.; Krugljak, Y. A. *Teor. Eksp. Khim* **1972**, *8*, 542.
(65) Ripoche, J. *Spectrochim. Acta* **1967**, *23A*, 1003.
(66) Grajcar, L.; Leach, S. *J. Chim. Phys.* **1964**, *61*, 1523.
(67) Varsanyi, G. *Assignments of 700 Benzene Derivatives*; Akademiai Kiadô: Budapest, 1973.
(68) Scip, R.; Schultz, G.; Hargittai, I.; Szabo, Z. G. *Z. Naturforsch.* **1977**, *32a*, 1178.
(69) Pang, F.; Boggs, J. E.; Pulay, P.; Forqarasi, G. *J. Mol. Struct.* **1980**, *66*, 281.
(70) Rossi, M.; Golden, D. M. *J. Am. Chem. Soc.* **1979**, *101*, 1230.
(71) Stull, D. R.; Westrum, E. F.; Sinke, G. G. *The Chemical Thermodynamics of Organic Compounds*; Wiley: New York, 1969.

Thermal Decomposition of Ethylbenzene, Styrene, and Bromophenylethane: UV Absorption Study in Shock Waves

W. Müller-Markgraf and J. Troe*

Institut für Physikalische Chemie der Universität Göttingen, Tammannstrasse 6, D-3400 Göttingen, West Germany *(Received: September 9, 1987; In Final Form: February 17, 1988)*

Shock wave studies of the pyrolysis of ethylbenzene, isopropylbenzene, *tert*-butylbenzene, styrene, and 1-bromo-1-phenylethane were performed using UV molecular absorption spectroscopy. By extensive spectral studies over the range 190–330 nm the overlapping absorption continua could be separated. Key observations in ethylbenzene pyrolysis were the dominance of a primary C–C bond split, the comparably fast fragmentation of benzyl radicals in agreement with observations from other benzyl sources, and the evidence for nonnegligible styrene formation. The following rate constants were derived: ethylbenzene → CH_3 + benzyl, $k_1 = 10^{15.55} \exp(-306.7 \text{ kJ mol}^{-1}/RT)\ s^{-1}$; styrene → benzene + acetylene, $k_{15} = 10^{11.2} \exp(-244.5 \text{ kJ mol}^{-1}/RT)\ s^{-1}$; 1-bromo-1-phenylethane → HBr + styrene, $k_{22} = 10^{12.5} \exp(-160 \text{ kJ mol}^{-1}/RT)\ s^{-1}$; benzyl fragmentation rates were identical with results from toluene, benzyl iodide, benzyl chloride, and other benzyl precursors. There is evidence for a dominant C–C bond split in isopropylbenzene and *tert*-butylbenzene pyrolysis as well.

Introduction

The pyrolysis of aromatic hydrocarbons has been studied extensively at moderate temperatures and the derived mechanisms are generally accepted today. Recent extensions of these investigations to high-temperature combustion conditions, however, have indicated a number of complications. Under these conditions fragmentations of radical species become fast enough to compete with radical recombination processes. As a consequence, the number of fast bimolecular reactions involving small radicals increases markedly and the mechanisms become more complex. In addition, dissociation processes can proceed on several channels. The described complications call for studies using all available analysis techniques. The various methods for following the reaction all have their advantages and limitations so that a series of complementary experiments is required. Recent studies of the pyrolysis of toluene, for example, have involved shock waves with laser schlieren, densitometry,[1] time-of-flight mass spectrometry,[1] UV molecular absorption,[2-6] atomic resonance absorption,[7-10] and

(1) Pamidimukkala, K. M.; Kern, R. D.; Patel, M. R.; Wei, H. C.; Kiefer, J. H. *J. Phys. Chem.* **1987**, *91*, 2148.
(2) Astholz, D. C.; Durant, J.; Troe, J. *Symp. (Int.) Combust., (Proc.), 18th* **1981**, 885.
(3) Astholz, D. C.; Troe, J. *J. Chem. Soc., Faraday Trans. 2* **1982**, *78*, 1413.
(4) Brouwer, L.; Müller-Markgraf, W.; Troe, J. *Symp. (Int.) Combust., (Proc.), 20th* **1984**, 799.
(5) Müller-Markgraf, W.; Troe, J. *Symp. (Int.) Combust., (Proc.), 21st* **1986**, 815.
(6) Brouwer, L.; Müller-Markgraf, W.; Troe, J. *J. Phys. Chem.*, preceding paper in this issue.
(7) Rao, V. S.; Skinner, G. B. *J. Phys. Chem.* **1984**, *88*, 4362.

0022-3654/88/2092-4914$01.50/0